PET/MRI: Reliability/Reproducibility of SUV Measurements

6

Habib Zaidi and Irene A. Burger

Contents

6.1 The Standardized Uptake Value (SUV) Metric

Qualitative visual interpretation of PET images is commonly performed to report abnormal tracer uptake in suspected regions. This is usually achieved by comparing observed patterns to expected normal biodistribution. However, the human visual system bears a number of limitations, and as such, this approach intrinsically suffers from intra- and interobserver variability owing to the subjective nature of visual interpretation [1]. Subsequently, guidelines on interpretation of PET images in clinical oncology advocated the adoption of simplified versions of PET metrics including semiquantitative indices, such as the standardized uptake value (SUV) [2].

H. Zaidi (✉)
Division of Nuclear Medicine and Molecular Imaging, Geneva University Hospital, Geneva, Switzerland
e-mail: Habib.Zaidi@hcuge.ch

I.A. Burger
Department of Nuclear Medicine, University Hospital Zurich, Zurich, Switzerland
e-mail: Irene.Burger@usz.ch

A. Iagaru et al. (eds.), *PET/MRI in Oncology*,
https://doi.org/10.1007/978-3-319-68517-5_6

Several methods for measuring PET tracer accumulation were proposed in the literature. The base is to measure the in vivo radioactivity concentration in the suspected malignant lesion (kBq/mL), which is directly linked to the tracer concentration. The two most significant sources of variation of tracer accumulation are the injected dose and the body weight representing whole-body distribution volume [1]. In practice, the SUV is calculated by dividing the decay-corrected activity concentration in the volume of interest (VOI) drawn around the lesion (MBq/mL) by the injected dose (MBq) divided by the body weight (g) [3]:

$$\mathrm{SUV} = \frac{\text{Mean ROI concentration}\left(\mathrm{MBq/mL}\right)}{\text{Injected dose}\left(\mathrm{MBq}\right)\Big/\text{Body weight}\left(\mathrm{g}\right)} \times \frac{1}{\text{decay factor}} \tag{6.1}$$

The SUV metric is widely used in the clinic because of its simplicity, ease of use, reproducibility, and compatibility with conventional whole-body PET/CT acquisition protocols, requiring only a static scan as opposed to full kinetic modeling approaches, which require complex dynamic studies and arterial blood sampling. Virtually all commercial and open-source medical image display software platforms offer the option to measure SUVs. However, considerable inconsistencies have been reported among the different software packages used in clinical and research settings as demonstrated in a recent study conducted by the PET technical committee of the Quantitative Imaging Biomarker Alliance initiative [4]. It should also be noted that most packages normalize SUV to patient's body weight (Eq. (6.1)). However, since adipose tissue is not as metabolically active as other tissues, other variants were suggested, including normalization to lean body mass ($\mathrm{SUV_{LBM}}$ or SUL) [5] or body surface area ($\mathrm{SUV_{BSA}}$) [6].

The maximum SUV ($\mathrm{SUV_{max}}$), representing the highest voxel SUV value, and mean SUV ($\mathrm{SUV_{mean}}$), representing the average SUV across all voxels in a defined VOI, are undoubtedly the most widely used semiquantitative metrics (Fig. 6.1). Conversely, $\mathrm{SUV_{peak}}$ (Fig. 6.1), defined in PERCIST criteria as representing the $\mathrm{SUV_{mean}}$ in a

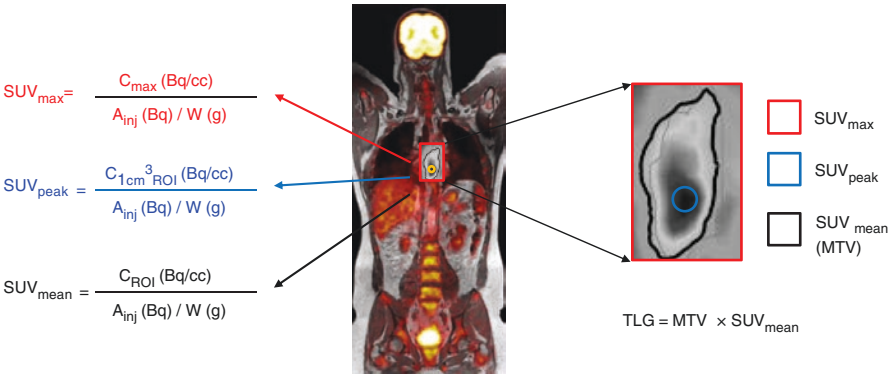

Fig. 6.1 Illustration of the basic foundations of PET quantification and the factors involved in the calculation of first- and second-order image-derived PET metrics used in clinical oncology

spherical VOI (1.2 cm diameter or 1 mL volume) placed over the most active part of a malignant lesion, was advocated as a more robust semiquantitative metric less vulnerable to artifacts [7]. Depending on the defined VOI, a variety of definitions of SUV_{peak} can be envisaged, obviously significantly affecting the resulting values [8].

6.2 Limitations of the SUV Metric

Despite its popularity and wide adoption in clinical and research settings, the SUV metric intrinsically bears a number of shortcomings which has limited its adoption in large clinical multicenter trials. The SUV also depends on the time course of the activity concentration in the blood plasma and the time point of acquisition and therefore imposes strict standardization of the uptake time, usually to 60 min with an acceptable range of 55–75 min according to the EANM guidelines 2015 [2]. Also the dependency of SUV on acquisition frame times, reconstruction parameters, physical and physiological factors, and scanner calibrations limits its potential in providing an objective assessment of whole-body PET images across baseline and follow-up studies for robust disease monitoring. Therefore, large multicenter clinical trials require standardization of data acquisition and processing protocols on different scanners for harmonization of PET quantification to enable pooling of data collected at different centers [9, 10].

To overcome the limitations of the SUV metric, alternative measures have been proposed including an uptake time-corrected version of the SUV including an uptake time quotient to normalize to 75 min [11] or simplified population-based blood pool activity-corrected estimations of FDG uptake, both trying to overcome the strong variability of SUV from uptake time and blood pool activity as approximations for more robust PET quantification [12]. The underlying principle for calculation of the glucose influx into the cell (MRGlu) was suggested about 25 years ago [13], but the fact that dynamic acquisition is needed did not render it feasible for whole-body imaging [14] until the advent of whole-body parametric imaging [15], which is now receiving considerable attention by the molecular imaging community. It can be anticipated that the additional information provided by parametric imaging through exploitation of the 4D spatiotemporal nature of the complete list-mode PET data, beyond the currently established semiquantitative SUV metric, might be valuable in whole-body PET imaging for multiparametric assessment of metastatic tumors across multiple beds and for improved reproducibility and evaluation of response to treatment over long periods [15].

Furthermore, volume-based PET metrics such as the total lesion glycolysis (TLG), calculated by multiplying SUV_{mean} by the metabolic tumor volume (MTV) [16], radiomic and texture analysis [17, 18], and parametric imaging have been suggested [14, 15]. The TLG, used to assess global metabolic response of the whole lesion thus providing complementary information to SUV and it variants, was shown to be highly correlated with other PET response parameters and is reproducible [19]. Recent advances in PET image segmentation and delineation of lesion contours [20] combined with progress in partial volume correction techniques have enabled to automate the calculation procedure. More recently, radiomics and texture

analysis emerged as new promising approaches enabling to circumvent the limitations of the above described oversimplified approaches by providing additional features including intratumoral heterogeneity through advanced image processing techniques and knowledge in systems biology [17, 18]. An increasing number of pioneering studies support the underlying assumptions of these hypotheses; however, further research and development efforts using large clinical databases are still required before these approaches can translate to valuable and reliable tools that can be adopted in the clinic.

6.3 Repeatability of SUV Measurements

A number of studies investigated the reproducibility of multiple PET metrics including $SUV_{max,}$ SUV_{mean}, TLG, and MTV. All publications conclude that PET metrics are reproducible [21], with an almost perfect interobserver agreement for SUV_{max} [22, 23]. Furthermore, numerous studies showed that SUV_{max} has a prognostic value and correlates with progression-free and overall survival [24, 25]. This led to the widespread use of SUV_{max} as predictive and prognostic value for oncology PET assessments supported by the recommendations of the European Association of Nuclear Medicine guidelines 1.0 for PET/CT [26]. Six years later, the updated version 2.0 still recommends reporting SUV_{max} with the addition of SUV_{peak} to quantify tumor activity. SUV_{peak} is using a 3D 1.2 cm diameter (and 1.0 mL volume) spherical VOI positioned such that the average value across all positions within the lesion is maximized [7]. This alternative measure of the highest activity within a tumor was introduced due to the major limitation of SUV_{max}, that is, the high variability introduced by the statistical noise associated with a single voxel analysis. As has been shown in phantom and dynamic patient studies, this statistical noise substantially impairs the repeatability of SUV_{max} [27–29]. Averaging the values of a number of voxels within a given VOI, as proposed by SUV_{peak} [30, 31], can reduce this noise and therefore increases the repeatability without significant reduction of reproducibility. Using SUV_{peak} rather than an averaged number of the hottest voxels in a VOI has the advantage of a standardized volume irrespective of reconstruction methods and voxel sizes. However, the absolute activity drops compared to an averaged number of the hottest voxels in a VOI since not all voxels within SUV_{peak} have a high activity, which might impair the discrimination between high-activity lesions [32].

6.4 Clinical Relevance of the SUV

The use of FDG PET for therapy response assessment and evaluation of tumor aggressiveness is increasing. Most publications using PERCIST 1.0 as the base for PET-based therapy response assessment for solid and nonsolid tumors are based on SUV_{max} or SUV_{peak} [7, 33, 34]. PERCIST 1.0 suggested a cutoff at 30% increase for progressive disease and 30% decrease for partial remission, which is a slight increase in difference compared to the 25% according to the 1999 EORTC recommendation. A study comparing both evaluation systems for response assessment in

metastatic colorectal cancer came to the conclusion that they were equivalent [35]; however, several studies comparing CT-based RECIST with FDG quantification found that PET was superior in predicting histopathological therapy response [36, 37], time to progression [38], or overall survival [39].

Besides the increasing use of FDG PET for therapy response assessment, baseline quantitative PET metrics are also increasingly used to predict outcome. Initially these were predominantly based on SUV_{max} [24, 25, 40]. However, more and more publications come to the conclusion that volume-based PET metrics, such as MTV or TLG, are superior prognostic markers on baseline PET scans compared to SUV_{max} [41–43].

For cardiac FDG-PET evaluation, the absolute SUV values are less important than the relative difference within the cardiac wall using polar maps normalized to the peak activity. Here a direct comparison of the relative activity in the 20 cardiac segments between PET/CT and PET/MR showed an excellent correlation between both modalities that was even slightly improved for PET/MR with time-of-flight (TOF) capability (mean -1.3%) compared to non-TOF PET/MR (mean -2.1%) [44].

Analog to cardiac PET, also quantification of neuro-PET is rather performed based on tumor-to-background (TBR) ratios than absolute SUV values. The first study comparing PET quantification between PET/CT and PET/MR was performed for ^{11}C-methionine PET for gliomas and ^{68}Ga-DOTATOC in meningiomas. The authors concluded that the computed TBR exhibited an excellent accordance between PET/MR and PET/CT systems, with a correlation coefficient of 0.98 and a mean relative error of 7.9% [45].

6.5 Clinical Studies Comparing SUV Measurements Between PET/CT and PET/MRI in Oncology

Since the introduction of fully integrated PET/MR systems, multiple studies have been published comparing quantitative and qualitative results between PET/CT and PET/MR. In most of these studies, a same-day protocol with a single injection was performed. The majority had a significant difference in uptake time between PET/CT (commonly injected 60 min after injection) and the secondary PET/MR scan (with uptake times from 135 min [46] up to 180 min [47]). Table 6.1 summarizes results of studies comparing SUVs estimated on PET/CT and PET/MR images. Despite the sometimes large differences between uptake times, most studies came to the conclusion that there was a high positive correlation for all SUV quantification metrics between both exams and that most of the differences were due to the variance in uptake time between both scans [44–48, 50, 51, 53, 54, 57, 59–61, 64]. In only two studies, some scans were performed on the PET/MR scanner first [52, 58], and in two studies, all PET/MR scans were performed before PET/CT [49, 56]. All other studies had a longer uptake time of 51–120 min (mean 81 min) for the PET/MR scans and showed a slight increase in SUV between both exams. Sher et al. performed 40 scans, 31 on the PET/MR system and 9 on the PET/CT first. They showed that SUV values were always higher on the second scan for malignant lesion further supporting that the observed difference in the other studies is rather due to the increasing uptake over time than different technology.

Table 6.1 Summary of results presented in the literature comparing SUVs estimated on PET/CT images to those measurements on PET/MR images

Authors (reference)	Year	Journal	Tracers	Patient number	PET/CT uptake	PET/MRI uptake	Indication	Scanner	Main conclusions
Boss et al. [45]	2010	JNM	^{11}C-methionine, ^{68}Ga-DOTATOC	10	60 min	90–120 min	Brain tumors	Biograph mMR	Tumor-to-reference tissue ratios with excellent correlation (0.98), with a mean relative error of 7.9%
Drzezga et al. [48]	2012	JNM	^{18}F-FDG	32	86 min	140 min	Cancer general	Biograph mMR	High correlation between mean SUVs on PET/MRI and PET/CT in lesions ($r = 0.93$) and background tissue ($r = 0.92$)
Varoquaux et al. [49]	2014	EJNMMI	^{18}F-FDG	32	146 min	85 min	Head and neck	Ingenuity TF PET/MR	Excellent correlation between SUVs on both modalities, with an underestimation on PET/MRI as compared to PET/CT
Kershah et al. [50]	2013	MIB	^{18}F-FDG	40	66 min	117 min	Cancer general	Ingenuity TF PET/MR	High correlation for SUV values obtained from PET/MRI compared to those from PET/CT, as the reference standard

Wiesmüller et al. [51]	2013	EJNMMI	^{18}F-FDG, ^{8}F-FEC, ^{68}Ga-D-TATE	43	60 min	140 min	Cancer general	Biograph mMR	Differences demonstrated in quantification of tracer uptake between PET/CT and PET/MRI were minor but statistically significant
Schäfer et al. [52]	2014	Radiology	^{18}F-FDG	20	60 min/118 min[a]	128 min/63 min[a]	Pediatrics	Biograph mMR	13.1% deviation of SUVs for bone marrow and 5% deviation for other tissues
Afshar-Oromich et al. [53]	2014	EJNMMI	^{68}Ga-PSMA	20	60 min	180 min	Prostate cancer	Biograph mMR	Scatter correction on PET/MRI challenging and direct comparison of SUVs from PET/CT and PET/MRI needs to be conducted carefully
Al-Nabhani et al. [46]	2014	JNM	^{18}F-FDG, ^{68}Ga-D-TATE, ^{18}F-FECH	50	56 min	135 min	Cancer general	Biograph mMR	PET data on both modalities were similar with significant correlation between mean SUVs

(continued)

Table 6.1 (continued)

Authors (reference)	Year	Journal	Tracers	Patient number	PET/CT uptake	PET/MRI uptake	Indication	Scanner	Main conclusions
Sachpekidis et al. [54]	2015	AJNMMI	^{18}F-FDG	30	60 min	120 min	Multiple myeloma	Biograph mMR	Significant correlation between the two techniques was demonstrated, despite the statistically significant differences in lesional SUVs between PET/CT and PET/MRI
Queiroz et al. [55]	2015	PLoS One	^{18}F-FDG	75	na	na	Cancer general	SIGNA PET/MR	TOF-PET/MRI device requires significantly less activity to generate PET images with good-to-excellent image quality
Lyons et al. [56]	2015	AJR	^{18}F-FDG	35	108 min	61 min	Pediatrics	Ingenuity TF PET/MR	Good correlation for SUV on both modalities, PET/MRI underestimated SUV compared with PET/CT

Vontobel et al. [44]	2015	EJNMMI	^{18}F-FDG	23	60 min	106 min	Cardiac	SIGNA PET/MR	PET/MRI with and without TOF showed minimal underestimation of tracer uptake (−2.08 and −1.29%, respectively), compared to PET/CT
Iagaru et al. [57]	2015	Clin Nucl Med	^{18}F-FDG	36	74 min	161 min	Cancer general	SIGNA PET/MR	The mean SUV_{max} values were higher in PET/MRI than PET/CT for all lesions
Sher et al. [58]	2016	AJR	^{18}F-FDG	40	90 min/132 min[b]	71 min/124 min	Pediatric lymphoma	Ingenuity TF PET/MR	PET/MRI quantification strongly correlated with PET/CT, but the SUVs were not interchangeable
Freitag et al. [47]	2016	EJNMMI	^{68}Ga-PSMA	26	60 min	180 min	Prostate cancer	Biograph mMR	The correlation between PET/MRI and PET/CT SUVs was linear in lymph nodes and bone metastases

(continued)

Table 6.1 (continued)

Authors (reference)	Year	Journal	Tracers	Patient number	PET/CT uptake	PET/MRI uptake	Indication	Scanner	Main conclusions
Sawicki et al. [59]	2016	JNM	^{18}F-FDG	121	61 min	113 min	Pulmonary nodules	Biograph mMR	Lesion size, SUV, and characterization correlate strongly between the two modalities
Atkinson et al. [60]	2016	Abdom Radiol	^{18}F-FDG	18	60 min	na	Lymphoma	Biograph mMR	SUV values were comparable with high positive correlation. Similar lesion detection rate
Xin et al. [61]	2016	Eur J Radiol	^{18}F-FDG	45	64 min	170 min	Abdominal/ pelvic	Ingenuity TF PET/ MR	High correlation between the two modalities in terms of SUV_{max} and SUV_{mean} in focal lesions
Karlberg et al. [62]	2016	EJNMMI Phys	^{18}F-FDG	Phantom	na	na	na	Biograph mMR	NECRs and sensitivity are higher for PET/ MRI. Differences in image quality are most evident for challenging settings. PET/CT performance better owing to TOF capability

Seith et al. [63]	2016	Invest Radiol	^{18}F-FDG, ^{68}Ga-DOTATATE, ^{11}C-choline	66	na	na	Cancer general	Biograph mMR	MRI-based AC is accurate in most tissues (SUV deviations generally <10%). Underestimations in the bone and overestimation close to the lung can be pronounced
Afaq et al. [64]	2017	Clin Nucl Med	^{18}F-FDG	68	64 min	136 min	Lymphoma	Biograph mMR	SUV_{max} correlated significantly with a correlation coefficient of 0.84
Law et al. [65]	2017	Clin Nucl Med	^{18}F-FDG	100	63 min	116 min	Cancer general	Biograph mMR	Excellent correlation between SUVs in lesions on PET/MRI and PET/CT, across all body regions and in all tumor types studied

[a]In four patients PET/MRI scans were performed before PET/CT
[b]For nine scans PET/CT before PET/MRI

To investigate the influence of MR-based attenuation correction (AC) on absolute SUV, Seith et al. used the same PET dataset from an integrated PET/MR scanner and reconstructed it either with the tissue segmentation-based MRAC μ-map or the CTAC μ-map using a nonrigid registration of the CT to the MR-based μ-map. They showed that MR-based AC is very accurate in most tissues with SUV deviations of generally <10%. A systematic underestimation of SUV was only present in the bones, while some lesions close to the lung were overestimated [63]. These results are in line with earlier published simulation data showing a significant decrease of up to 30% in sclerotic lesion, after subtraction of all voxels with bone density from the CTAC μ-map (Fig. 6.3) [38].

A quantitative phantom study comparing image quality between TOF PET/CT (Siemens Biograph mCT) and non-TOF PET/MR (Siemens Biograph mMR) showed that the spatial resolution was similar for the two systems. Average sensitivity was higher for the mMR (13.3 kcps/MBq) compared to the mCT system (10.0 kcps/MBq), and peak noise equivalent count rate (NECR) was slightly higher for the mMR (196 kcps @ 24.4 kBq/mL) compared to the mCT (186 kcps @ 30.1 kBq/mL). Highest hot contrast for the smallest sphere (10 mm) was achieved with the combination of TOF and PSF on the mCT compared to the mMR. Overall the differences between both systems were mainly due to the TOF possibility on the mCT, which resulted in an overall better image quality, especially for the more challenging settings with higher background activity and small uptake volumes [62]. For the fully integrated PET/MR scanner with TOF, only a few studies were published comparing PET quantification on PET/CT and PET/MR until today [44, 55, 57]. A prospective trial comparing TOF PET/CT (Discovery D 690 PET/CT, GE Healthcare) and TOF PET/MR (SIGNA PET/MR) in 75 patients based on phantom NECR curves investigated the potential dose reduction for PET/MR with equivalent image quality. They concluded that a reduction of FDG activity of slightly more the 50% can be achieved thanks to improvements in detector geometry and technologies [55].

6.6 Reliability of SUV Measurements in PET/MRI

The challenges faced by quantitative PET/CT imaging have been investigated since the commercial availability of this technology more than 15 years ago, and several professional societies established committees and task groups (e.g., QIBA/RSNA, CQIE/ACRIN, QIN/AAPM, etc.) to support and promote the use of quantitative imaging biomarkers in the context of cancer staging and therapy response assessment. The deployment of hybrid PET/MRI in the clinic poses new challenges and additional difficulties to enable reliable, quantitative imaging biomarkers. The primary challenge is the lack of a robust MRI-guided attenuation correction particularly in whole-body imaging. Furthermore, partial volume and motion correction need to be considered to produce artifact-free and quantitative PET images, with robust and reliable quantitative indices for routine application and advanced tools for clinical and research applications. The bulk of quantitative PET/MRI research to date focused on addressing the challenges of MRI-guided PET attenuation correction. Three categories of MRI-guided attenuation correction techniques have emerged [66]. This

includes (1) segmentation-based approaches, which segment MR images into different tissue classes and assign predefined attenuation coefficients to each class, (2) atlas-based and machine learning techniques in which co-registered MR-CT Atlas pairs are used to derive a pseudo-CT image or to learn a mapping function that predicts the pseudo-CT from actual patient's MRI, and (3) the recently revisited joint emission and attenuation reconstruction algorithms or maximum likelihood reconstruction of attenuation and activity (MLAA), in which the attenuation map is estimated from emission or transmission data. Figure 6.2 shows a representative clinical FDG brain PET study comparing various attenuation correction strategies.

Segmented MRI-guided attenuation correction widely used on commercial PET/MRI systems suffers the lack of bones in the derived attenuation map, which induces underestimation of the SUV in the corresponding regions within or close

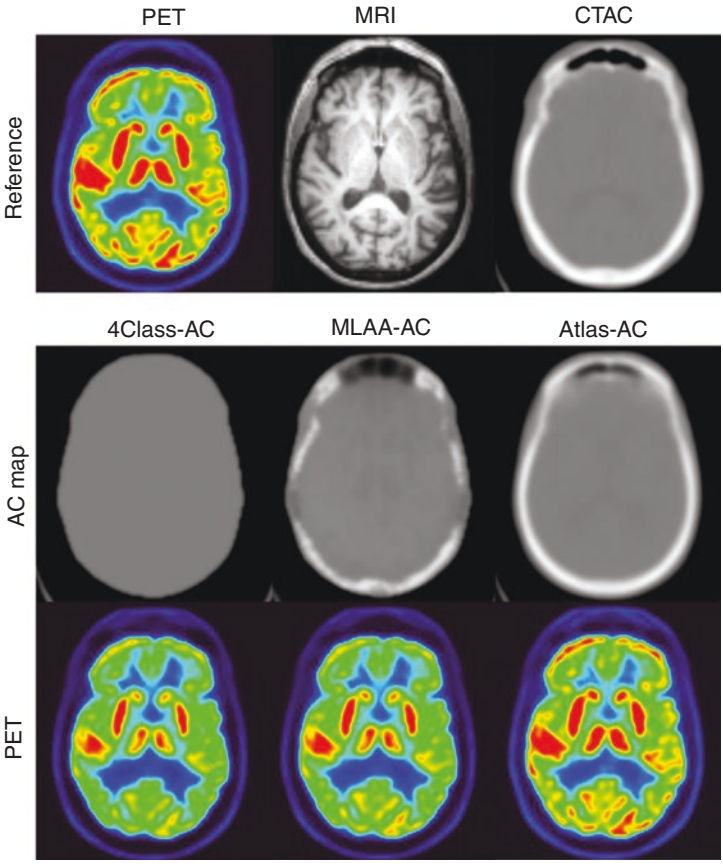

Fig. 6.2 Representative clinical FDG brain PET study showing from left to right: (top row) PET, MR, and CT images used as reference for evaluation, (middle row) attenuation maps derived using different attenuation correction approaches including segmented MRI, Atlas-guided, and maximum likelihood reconstruction of attenuation and activity (MLAA) technique, (bottom row) corresponding reconstructed PET images. Note the limitations of segmented MRI-based approach which ignores the skull and air cavities. The Atlas-based approach better matches the patient's CT image, clearly outperforming the MLAA algorithm

to the bones on PET images (Fig. 6.3) [67, 68]. Likewise, metal artifacts can lead to substantial signal voids and underestimation of SUV. This can be compensated by exploiting TOF reconstruction [69, 70], which was shown to reduce the SUV bias compared to non-TOF-PET emission data [71, 72]. Further improvement is possible with the joint emission-transmission reconstruction algorithm which showed promise in the correction of metal susceptibility artifacts by estimating the high attenuation coefficients of metallic implants [73]. Furthermore, the development of appropriate MR sequences, such as multi-acquisition variable-resonance image combination (MAVRIC) [74], can reduce metal artifacts. An additional complexity arises from the attenuation and scattering of annihilation photons by objects present in the field of view, which may also induce SUV underestimation if not accounted for. This includes patient's bed, MRI radiofrequency body or surface coils, and patient positioning aids [66]. Transmission or CT scanning-based predetermination of attenuation maps for rigid objects (bed, body coils, etc.) and nonrigid registration of templates of flexible objects (surface coils) [75] is currently used to account for the additional attenuation from these items. Joint reconstruction of emission and transmission images was purportedly promoted as potential approach enabling to estimate the attenuation maps of these objects. However, the performance of this approach for recovering objects lacking support from emission data remains to be demonstrated in clinical setting.

6.7 Summary

Objective quantification of PET tracer uptake is gaining significance with the increasing use of PET as a prognostic biomarker for therapy response assessment. Ease of use, availability, as well as excellent reproducibility and correlation with

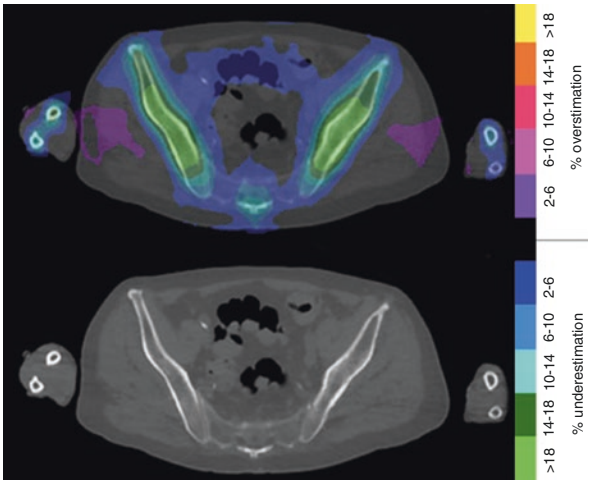

Fig. 6.3 Relative difference between PET images reconstructed with and without considering bony structures on CTAC attenuation map with the corresponding axial CT image

tumor aggressiveness lead to widespread use of SUV_{max} for tumor assessment, despite its well-known limitations, such as high variability with uptake time, blood pool activity, and limited repeatability.

With PET/MRI as a new hybrid modality being now commercially available, additional challenges are faced for reliable PET quantification. Although numerous studies showed an overall high correlation among SUV measurements between PET/CT and PET/MR, impaired attenuation correction due to the missing density of bone and metal implants can substantially affect SUV values within the bones and adjacent structures. More research and development efforts are required to improve MRI-based attenuation correction using machine learning algorithms to create a pseudo-CT or through advanced priors for joint estimation of emission, and attenuation using TOF-PET data to correct the attenuation map is currently ongoing and will further improve reliable PET quantification for PET/MRI.

Acknowledgments This work was supported by the Swiss National Science Foundation under Grant SNSF 31003A-149957 and the Swiss Cancer Research Foundation under Grant KFS-3855-02-2016.

References

1. Basu S, Zaidi H, Houseni M, et al. Novel quantitative techniques for assessing regional and global function and structure based on modern imaging modalities: implications for normal variation, aging and diseased states. Semin Nucl Med. 2007;37:223–39.
2. Boellaard R, Delgado-Bolton R, Oyen WJ, et al. FDG PET/CT: EANM procedure guidelines for tumour imaging: version 2.0. Eur J Nucl Med Mol Imaging. 2015;42:328–54.
3. Huang SC. Anatomy of SUV. Standardized uptake value. Nucl Med Biol. 2000;27:643–6.
4. Pierce LA II, Elston BF, Clunie DA, Nelson D, Kinahan PE. A digital reference object to analyze calculation accuracy of PET standardized uptake value. Radiology. 2015;277:538–45.
5. Zasadny KR, Wahl RL. Standardized uptake values of normal tissues at PET with 2-[fluorine-18]-fluoro-2-deoxy-D-glucose: variations with body weight and a method for correction. Radiology. 1993;189:847–50.
6. Kim CK, Gupta NC, Chandramouli B, Alavi A. Standardized uptake values of FDG: body surface area correction is preferable to body weight correction. J Nucl Med. 1994;35:164–7.
7. Wahl RL, Jacene H, Kasamon Y, Lodge MA. From RECIST to PERCIST: evolving considerations for PET response criteria in solid tumors. J Nucl Med. 2009;50:122S–150.
8. Vanderhoek M, Perlman SB, Jeraj R. Impact of the definition of peak standardized uptake value on quantification of treatment response. J Nucl Med. 2012;53:4–11.
9. Boellaard R. Optimisation and harmonisation: two sides of the same coin? Eur J Nucl Med Mol Imaging. 2013;40:982–4.
10. Sunderland JJ, Christian PE. Quantitative PET/CT scanner performance characterization based upon the society of nuclear medicine and molecular imaging clinical trials network oncology clinical simulator phantom. J Nucl Med. 2015;56:145–52.
11. Hofheinz F, Apostolova I, Oehme L, Kotzerke J, van den Hoff J. Test-retest variability of lesion SUV and lesion SUR in 18F-FDG PET: an analysis of data from two prospective multicenter trials. J Nucl Med. 2017. https://doi.org/10.2967/jnumed.117.190736.
12. Burger IA, Burger C, Berthold T, Buck A. Simplified quantification of FDG metabolism in tumors using the autoradiographic method is less dependent on the acquisition time than SUV. Nucl Med Biol. 2011;38:835–41.

13. Patlak CS, Blasberg RG, Fenstermacher JD. Graphical evaluation of blood-to-brain transfer constants from multiple-time uptake data. J Cereb Blood Flow Metab. 1983;3:1–7.
14. Dimitrakopoulou-Strauss A, Pan L, Strauss LG. Parametric imaging: a promising approach for the evaluation of dynamic PET-18F-FDG studies – the DKFZ experience. Hell J Nucl Med. 2010;13:18–22.
15. Karakatsanis NA, Casey ME, Lodge MA, Rahmim A, Zaidi H. Whole-body direct 4D parametric PET imaging employing nested generalized Patlak expectation-maximization reconstruction. Phys Med Biol. 2016;61:5456–85.
16. Larson SM, Erdi Y, Akhurst T, et al. Tumor treatment response based on visual and quantitative changes in global tumor glycolysis using PET-FDG imaging. The visual response score and the change in total lesion glycolysis. Clin Positron Imaging. 1999;2:159–71.
17. Yip SS, Aerts HJ. Applications and limitations of radiomics. Phys Med Biol. 2016;61:R150–66.
18. Hatt M, Tixier F, Pierce L, et al. Characterization of PET/CT images using texture analysis: the past, the present… any future? Eur J Nucl Med Mol Imaging. 2017;44:151–65.
19. Houshmand S, Salavati A, Hess S, et al. An update on novel quantitative techniques in the context of evolving whole-body PET imaging. PET Clin. 2015;10:45–58.
20. Hatt M, Lee J, Schmidtlein CR, et al. Classification and evaluation strategies of auto-segmentation approaches for PET: report of AAPM task group no. 211. Med Phys. 2017;44(6):e1–e42.
21. Weber WA, Ziegler SI, Thodtmann R, Hanauske AR, Schwaiger M. Reproducibility of metabolic measurements in malignant tumors using FDG PET. J Nucl Med. 1999;40:1771–7.
22. Benz MR, Evilevitch V, Allen-Auerbach MS, et al. Treatment monitoring by 18F-FDG PET/CT in patients with sarcomas: interobserver variability of quantitative parameters in treatment-induced changes in histopathologically responding and nonresponding tumors. J Nucl Med. 2008;49:1038–46.
23. Jacene HA, Leboulleux S, Baba S, et al. Assessment of interobserver reproducibility in quantitative 18F-FDG PET and CT measurements of tumor response to therapy. J Nucl Med. 2009;50:1760–9.
24. Kidd EA, Siegel BA, Dehdashti F, Grigsby PW. The standardized uptake value for F-18 fluorodeoxyglucose is a sensitive predictive biomarker for cervical cancer treatment response and survival. Cancer. 2007;110:1738–44.
25. Pandit N, Gonen M, Krug L, Larson SM. Prognostic value of [18F]FDG-PET imaging in small cell lung cancer. Eur J Nucl Med Mol Imaging. 2003;30:78–84.
26. Boellaard R, O'Doherty MJ, Weber WA, et al. FDG PET and PET/CT: EANM procedure guidelines for tumour PET imaging: version 1.0. Eur J Nucl Med Mol Imaging. 2010;37:181–200.
27. Burger IA, Huser DM, Burger C, von Schulthess GK, Buck A. Repeatability of FDG quantification in tumor imaging: averaged SUVs are superior to SUVmax. Nucl Med Biol. 2012;39:666–70.
28. de Langen AJ, Vincent A, Velasquez LM, et al. Repeatability of 18F-FDG uptake measurements in tumors: a metaanalysis. J Nucl Med. 2012;53:701–8.
29. Schwartz J, Humm JL, Gonen M, et al. Repeatability of SUV measurements in serial PET. Med Phys. 2011;38:2629–38.
30. Akamatsu G, Ikari Y, Nishida H, et al. Influence of statistical fluctuation on reproducibility and accuracy of SUVmax and SUVpeak: a phantom study. J Nucl Med Technol. 2015;43:222–6.
31. Lodge MA, Chaudhry MA, Wahl RL. Noise considerations for PET quantification using maximum and peak standardized uptake value. J Nucl Med. 2012;53:1041–7.
32. Laffon E, Lamare F, de Clermont H, Burger IA, Marthan R. Variability of average SUV from several hottest voxels is lower than that of SUVmax and SUVpeak. Eur Radiol. 2014;24:1964–70.
33. Hyun OJ, Luber BS, Leal JP, et al. Response to early treatment evaluated with F-18-FDG PET and PERCIST 1.0 predicts survival in patients with ewing sarcoma family of tumors treated with a monoclonal antibody to the insulinlike growth factor 1 receptor. J Nucl Med. 2016;57:735–40.
34. Pinker K, Riedl CC, Ong L, et al. The impact that number of analyzed metastatic breast cancer lesions has on response assessment by F-18-FDG PET/CT using PERCIST. J Nucl Med. 2016;57:1102–4.

35. Skougaard K, Nielsen D, Jensen BV, Hendel HW. Comparison of EORTC criteria and PERCIST for PET/CT response evaluation of patients with metastatic colorectal cancer treated with irinotecan and cetuximab. J Nucl Med. 2013;54:1026–31.
36. Burger IA, Casanova R, Steiger S, et al. 18F-FDG PET/CT of non-small cell lung carcinoma under neoadjuvant chemotherapy: background-based adaptive-volume metrics outperform TLG and MTV in predicting histopathologic response. J Nucl Med. 2016;57:849–54.
37. Denecke T, Rau B, Hoffmann KT, et al. Comparison of CT, MRI and FDG-PET in response prediction of patients with locally advanced rectal cancer after multimodal preoperative therapy: is there a benefit in using functional imaging? Eur Radiol. 2005;15:1658–66.
38. Kanemura S, Kuribayashi K, Funaguchi N, et al. Metabolic response assessment with 18F-FDG-PET/CT is superior to modified RECIST for the evaluation of response to platinum-based doublet chemotherapy in malignant pleural mesothelioma. Eur J Radiol. 2017;86:92–8.
39. Yoon JW, Kim S, Kim SW, et al. PET/CT response criteria (European Organization for Research and Treatment of cancer) predict survival better than response evaluation criteria in solid tumors in locally advanced cervical cancer treated with chemoradiation. Clin Nucl Med. 2016;41:677–82.
40. Borst GR, Belderbos JS, Boellaard R, et al. Standardised FDG uptake: a prognostic factor for inoperable non-small cell lung cancer. Eur J Cancer. 2005;41:1533–41.
41. Chung HW, Lee KY, Kim HJ, Kim WS, So Y. FDG PET/CT metabolic tumor volume and total lesion glycolysis predict prognosis in patients with advanced lung adenocarcinoma. J Cancer Res Clin Oncol. 2014;140:89–98.
42. Hyun SH, Ahn HK, Kim H, et al. Volume-based assessment by (18)F-FDG PET/CT predicts survival in patients with stage III non-small-cell lung cancer. Eur J Nucl Med Mol Imaging. 2014;41:50–8.
43. Lee JW, Kang CM, Choi HJ, et al. Prognostic value of metabolic tumor volume and total lesion glycolysis on preoperative (1)(8)F-FDG PET/CT in patients with pancreatic cancer. J Nucl Med. 2014;55:898–904.
44. Vontobel J, Liga R, Possner M, et al. MR-based attenuation correction for cardiac FDG PET on a hybrid PET/MRI scanner: comparison with standard CT attenuation correction. Eur J Nucl Med Mol Imaging. 2015;42:1574–80.
45. Boss A, Bisdas S, Kolb A, et al. Hybrid PET/MRI of intracranial masses: initial experiences and comparison to PET/CT. J Nucl Med. 2010;51:1198–205.
46. Al-Nabhani KZ, Syed R, Michopoulou S, et al. Qualitative and quantitative comparison of PET/CT and PET/MR imaging in clinical practice. J Nucl Med. 2014;55:88–94.
47. Freitag MT, Radtke JP, Hadaschik BA, et al. Comparison of hybrid (68)Ga-PSMA PET/MRI and (68)Ga-PSMA PET/CT in the evaluation of lymph node and bone metastases of prostate cancer. Eur J Nucl Med Mol Imaging. 2016;43:70–83.
48. Drzezga A, Souvatzoglou M, Eiber M, et al. First clinical experience with integrated whole-body PET/MR: comparison to PET/CT in patients with oncologic diagnoses. J Nucl Med. 2012;53:845–55.
49. Varoquaux A, Rager O, Poncet A, et al. Detection and quantification of focal uptake in head and neck tumours: (18)F-FDG PET/MR versus PET/CT. Eur J Nucl Med Mol Imaging. 2014;41:462–75.
50. Kershah S, Partovi S, Traughber BJ, et al. Comparison of standardized uptake values in normal structures between PET/CT and PET/MRI in an oncology patient population. Mol Imaging Biol. 2013;15:776–85.
51. Wiesmuller M, Quick HH, Navalpakkam B, et al. Comparison of lesion detection and quantitation of tracer uptake between PET from a simultaneously acquiring whole-body PET/MR hybrid scanner and PET from PET/CT. Eur J Nucl Med Mol Imaging. 2013;40:12–21.
52. Schafer JF, Gatidis S, Schmidt H, et al. Simultaneous whole-body PET/MR imaging in comparison to PET/CT in pediatric oncology: initial results. Radiology. 2014;273:220–31.
53. Afshar-Oromieh A, Haberkorn U, Schlemmer HP, et al. Comparison of PET/CT and PET/MRI hybrid systems using a 68Ga-labelled PSMA ligand for the diagnosis of recurrent prostate cancer: initial experience. Eur J Nucl Med Mol Imaging. 2014;41:887–97.
54. Sachpekidis C, Hillengass J, Goldschmidt H, et al. Comparison of (18)F-FDG PET/CT and PET/MRI in patients with multiple myeloma. Am J Nucl Med Mol Imaging. 2015;5:469–78.

55. Queiroz MA, Delso G, Wollenweber S, et al. Dose optimization in TOF-PET/MR compared to TOF-PET/CT. PLoS One. 2015;10:e0128842.
56. Lyons K, Seghers V, Sorensen JI, et al. Comparison of standardized uptake values in normal structures between PET/CT and PET/MRI in a tertiary pediatric hospital: a prospective study. AJR Am J Roentgenol. 2015;205:1094–101.
57. Iagaru A, Mittra E, Minamimoto R, et al. Simultaneous whole-body time-of-flight 18F-FDG PET/MRI: a pilot study comparing SUVmax with PET/CT and assessment of MR image quality. Clin Nucl Med. 2015;40:1–8.
58. Sher AC, Seghers V, Paldino MJ, et al. Assessment of sequential PET/MRI in comparison with PET/CT of pediatric lymphoma: a prospective study. AJR Am J Roentgenol. 2016;206:623–31.
59. Sawicki LM, Grueneisen J, Buchbender C, et al. Comparative performance of (1)(8)F-FDG PET/MRI and (1)(8)F-FDG PET/CT in detection and characterization of pulmonary lesions in 121 oncologic patients. J Nucl Med. 2016;57:582–6.
60. Atkinson W, Catana C, Abramson JS, et al. Hybrid FDG-PET/MR compared to FDG-PET/CT in adult lymphoma patients. Abdom Radiol (NY). 2016;41:1338–48.
61. Xin J, Ma Q, Guo Q, et al. PET/MRI with diagnostic MR sequences vs PET/CT in the detection of abdominal and pelvic cancer. Eur J Radiol. 2016;85:751–9.
62. Karlberg AM, Saether O, Eikenes L, Goa PE. Quantitative comparison of PET performance-siemens biograph mCT and mMR. EJNMMI Phys. 2016;3:5.
63. Seith F, Gatidis S, Schmidt H, et al. Comparison of positron emission tomography quantification using magnetic resonance- and computed tomography-based attenuation correction in physiological tissues and lesions: a whole-body positron emission tomography/magnetic resonance study in 66 patients. Investig Radiol. 2016;51:66–71.
64. Afaq A, Fraioli F, Sidhu H, et al. Comparison of PET/MRI with PET/CT in the evaluation of disease status in lymphoma. Clin Nucl Med. 2017;42:e1–7.
65. Law WP, Maggacis N, Jeavons SJ, Miles KA. Concordance of 18F-FDG PET uptake in tumor and normal tissues on PET/MRI and PET/CT. Clin Nucl Med. 2017;42:180–6.
66. Mehranian A, Arabi H, Zaidi H. Vision 20/20: magnetic resonance imaging-guided attenuation correction in PET/MRI: challenges, solutions, and opportunities. Med Phys. 2016;43:1130–55.
67. Samarin A, Burger C, Wollenweber SD, et al. PET/MR imaging of bone lesions--implications for PET quantification from imperfect attenuation correction. Eur J Nucl Med Mol Imaging. 2012;39:1154–60.
68. Arabi H, Rager O, Alem A, et al. Clinical assessment of MR-guided 3-class and 4-class attenuation correction in PET/MR. Mol Imaging Biol. 2015;17:264–76.
69. Davison H, Ter Voert EE, de Galiza Barbosa F, Veit-Haibach P, Delso G. Incorporation of time-of-flight information reduces metal artifacts in simultaneous positron emission tomography/magnetic resonance imaging: a simulation study. Investig Radiol. 2015;50:423–9.
70. Ter Voert EE, Veit-Haibach P, Ahn S, et al. Clinical evaluation of TOF versus non-TOF on PET artifacts in simultaneous PET/MR: a dual centre experience. Eur J Nucl Med Mol Imaging. 2017;44(7):1223–33.
71. Mehranian A, Zaidi H. Impact of time-of-flight PET on quantification errors in MRI-based attenuation correction. J Nucl Med. 2015;56:635–41.
72. Delso G, Khalighi M, Ter Voert E, et al. Effect of time-of-flight information on PET/MR reconstruction artifacts: comparison of free-breathing versus breath-hold MR-based attenuation correction. Radiology. 2017;282:229–35.
73. Fuin ND, Pedemonte SD, Catalano OA, et al. PET/MR imaging in the presence of metal implants: completion of the attenuation map from PET emission data. J Nucl Med. 2017;58:840–5.
74. Gunzinger J, Delso G, Boss A, et al. Metal artifact reduction in patients with dental implants using multispectral three-dimensional data acquisition for hybrid PET/MRI. EJNMMI Phys. 2014;1:102.
75. Kartmann R, Paulus DH, Braun H, et al. Integrated PET/MR imaging: automatic attenuation correction of flexible RF coils. Med Phys. 2013;40:082301–14.